Subpicosecond Transient Absorption of Donor−Acceptor Biphenyls. Intramolecular Control of the Excited State Charge Transfer Processes by a Weak Electronic Coupling

Michael Maus,[†] Wolfgang Rettig,*[,†] Gediminas Jonusauskas,[‡] René Lapouyade,[§] and Claude Rullière*[,‡]

Institute of Physical and Theoretical Chemistry, Humboldt Universität zu Berlin, Bunsenstr. 1, 10117 Berlin, Germany, Centre de Physique Moléculaire Optique et Hertzienne, U.A. CNRS 283, Université de Bordeaux I, 351 cours de la Libération, 33405 Talence Cedex, France, and Laboratoire de Sciences Moléculaires, Institut de chimie de la Matière Condensée de Bordeaux, Avenue du Dr A. Schweitzer, 33608 Pessac Cedex, France

Received: April 8, 1998; In Final Form: June 19, 1998

The photoinduced intramolecular charge transfer processes of three differently twisted 4-(dimethylamino)-4′-cyanobiphenyl derivatives (**I**−**III**) have been investigated using time-resolved transient absorption and gain spectroscopy in the subpicosecond range. Independent of twist angle and solvent polarity, the kinetics and spectral evolutions after excitation clearly reveal a precursor−sater relationship for the electron transfer from a less emissive state of mixed ^1L_b/CT character to a highly emissive charge transfer (^{1}CT) state. Beside the occurrence of dual fluorescence gain, two transient absorption bands for the ^{1}CT state and one for the precursor state (^{1}FC) are observed. All bands are assigned to electronic transitions and correlated for all solvents and compounds. The band intensities are discussed with solvent polarity and twist angle controlled mixing between the charge transfer state ^{1}CT and the higher lying ^1L_b and ^1L_a states. In acetonitrile, the transient spectra of the pretwisted donor−acceptor biphenyl **III**, in contrast to the planar **I** and **II**, can be approximated by the sum of cation and anion spectra of the subunits demonstrating decoupled moieties. The kinetics of the CT processes are not dominated by solvation dynamics alone. As an example, in acetonitrile, ($\tau_l = 0.2$ ps, $\tau_s < 1$ ps) the kinetics are slower than 2.5 ps. The involvement of a weak electronic coupling matrix element is favored as a source for the intramolecular control of the CT reactions. Furthermore, for the strongly twisted biphenyl derivative **III**, a secondary intramolecular process to a more relaxed species (CTR) occurs after the initial CT step, in agreement with fluorescence studies.

1. Introduction

Photoinduced intramolecular electron transfer (ET) processes in biaryl systems have been extensively studied by a large number of groups.[1−15] ET dynamics in solution are determined by an interplay of solvation and intramolecular modes leading to two borderline cases (A) solvent control and (B) intramolecular control.

In the case of an adiabatic ET reaction with a negligible activation barrier (case A), it is generally accepted that the ET rate is strongly correlated to the solvent relaxation time τ_s.[5,6,16−21] In particular, for the biaryl system 9,9′ bianthryl (BA) in polar aprotic solvents, though no agreement with the longitudinal relaxation times τ_l exists, quantitative agreement for the ET rate with the inverse solvent relaxation time τ_s was observed mainly by Barbara and co-workers.[5,6,20] On the other hand, some molecular systems are known to deviate strongly from the correlation of the solvent dynamics with the observed ET rates (case B) and the adiabacity of these reactions is always a point of discussion. As an example, the photoinduced ET in 4-(9-anthryl)-*N*,*N*-dimethylaniline (ADMA) has been explained by the superposition of a very fast ET in the nonadiabatic regime with an adiabatic solvent-controlled ET.[8] An ET reaction much slower than the solvent relaxation times has experimentally been shown for 4-*N*,*N*-dimethylamino-benzonitrile (DMABN) in aprotic solvents.[22−24] Interestingly, new results[7] of BA in nitriles suggest that the torsional relaxation toward a more planar structure is slower than τ_s, which is in accordance with molecular dynamics calculations.[25] In the second group of ET reactions (case B) intramolecular dynamics, such as large-amplitude motions, crossing of a thermal barrier or transitions connected with weak coupling matrix elements are rate determining instead of the solvent control (case A).

Different models have been applied to explain the dependence of such ET kinetics on intramolecular and solvent parameters. Early models from Sumi, Nadler, and Marcus[26,27] did not yet take into account intramolecular quantum mechanical high-frequency modes, which have subsequently been treated in different extensions of these models.[28,29] In contrast to the purely classical model, the extended models were capable to explain observed rapid rates in slowly relaxing solvents with a change from solvent to vibrational control. Moreover, the importance of intramolecular vibrational modes of ET reactions especially in the Marcus inverted region has been substantiated by a number of recent experiments.[29−31] Theoretical approaches including large structural relaxations have been developed within two-dimensional stochastic treatments.[32−34] The model of Nordio predicts that the ratio of viscous to dielectric relaxation rate of the system is a key parameter and can lead either to solvent or to viscosity control.[34] Maroncelli[35] and Hynes[33] often accentuate that τ_s is only a simplified value for a distribution of solvent relaxation times and that fast inertial components of solvent motions are able to accelerate ET reactions. However,

[†] Institute of Physical and Theoretical Chemistry.
[‡] Centre de Physique Moléculaire Optique et Hertzienne.
[§] Laboratoire de Sciences Moléculaires.

S1089-5639(98)01768-X CCC: $15.00
Published on Web 08/26/1998

kinetic investigations on a particular molecular system are seldomly paired with a detailed analysis of the electronic structure.

ET reactions mainly occur on the femtosecond (fs) and picosecond (ps) time scales, and the progressive development of ultrafast spectroscopic experiments now allows very precise measurements of the rates. Thus, a number of recent ultrafast time-resolved studies on classical laser dyes,[36−40] which have frequently been used as probe molecules of solvation before,[35] suggest that the observed photodynamics are insufficiently described by a simple one-state kinetic model associated with ET occurring on the time scale of solvation (case A). A more appropriate description for these dyes seems to be that the ET reaction occurs in a precursor−sater relationship of two (or more) distinct species with different spectral and electronic properties evolving independently of solvation (case B). However, the spectral changes during the ET process are not very pronounced such that controversial discussions can be found regarding the question whether the temporal change is due to fast solvation components[35,41] (case A) or due to multiple excited states[39,41] (case B). A detailed electronic characterization of the precursor state is frequently missing in the literature.

To differentiate between the two cases A and B and to determine the states involved in the ET, time-resolved experiments on molecular systems with known electronic structure are necessary. A powerful tool is time-resolved transient absorption because it allows probing both ET kinetics as well as the electronic structure of the excited singlet states concerned. As intramolecular ET model systems we apply the series of differently twisted donor−acceptor biphenyls **I**−**III** possessing a structure with obvious donor and acceptor moieties which are directly linked in a varying spatial arrangement (see Scheme 1).

SCHEME 1: Molecular Structures of Donor−Acceptor Biphenyls Investigated and Corresponding Ground-state Twist Angles Derived from AM1 Calculations for the Gas Phase

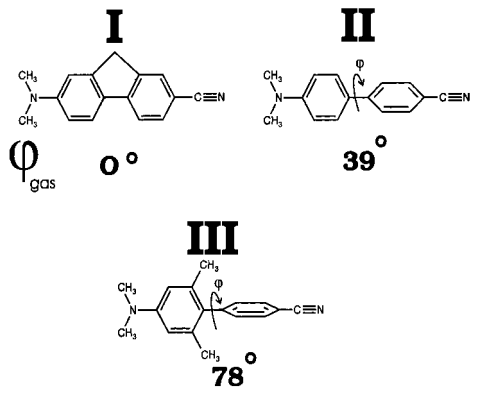

From our previous investigations,[3,4] it is known that these biphenyl compounds possess a close lying ^1L_b-type state above the low lying intramolecular charge-transfer S_1 state (^{1}CT). Fluorescence observed in the time range slower than 0.1 nanoseconds (ns) reveals only this intramolecular ^{1}CT state independently on excitation or emission wavelength as well as solvent and temperature.[1,2,4,9,10] Lahmani et al. recently reported that the charge-transfer process in **II** is governed only by solvation[2] because the observed decay kinetics in alcohols occur on the time scale of solvent relaxation. But the resolution of their setup (30 ps) was too limited to observe an electron transfer that might be complete prior to solvent reorganization. With the subpicosecond setup used here (time resolution of 1 ps) we aimed to search for a possible initial relaxation.

The key question for the transient absorption experiments is whether the initially populated state after vibrational relaxation, which will be termed as the (relaxed) Franck−Condon species **FC**, is of the same electronic nature as the ^{1}CT state or not. In other words, do we have to take into account only one state $S_1(2^1A)$ that changes its charge transfer chararacter gradually on the time scale of the solvent relaxation (case A) or are two distinct states involved (case B), the first one with locally excited character transforming into the second one with charge transfer character? In the one-state model, there should only be a continuous blue shift of the transient absorption bands on the time scale of solvation. However, if the two-state model is more appropriate, we should see different spectra of a first and a second species which are not necessarily transforming gradually on the time scale of the solvent relaxation τ_s. Moreover, a decay and rise behavior of the kinetics should be observable.

2. Experimental Section

2.1. Materials. The synthesis of the compounds **I**−**III** is described elsewhere.[4] The solvents *n*-hexane (HEX), diethyl ether (EOE), and acetonitrile (ACN) were of spectroscopic grade (Merck UVASOL). Triacetine (or glycerol triacetate, TAC), as purchased from Merck, has been washed with Na_2CO_3 and afterward distilled twice under vacuum shortly before use. The optical density (OD) for all solutions was adjusted to OD = 1.0 in a 1 cm cuvette at the fixed pump energy of 33300 cm^{-1} (300 nm) yielding concentrations lower than 1.7×10^{-4} M (for **III** in triacetine and acetonitrile the optical density was slightly higher because of a too small transient signal under these conditions).

2.2. Picosecond Pump−Probe Experiments. The experimental setup has been described in detail elsewhere.[42] Briefly, the laser system is based on a hybridly mode-locked dye laser (Coherent 702), synchronously pumped by a cw mode-locked Nd^{3+}/YAG laser (Coherent "ANTARES"), and the light emitted is amplified in a three stage dye amplifier (Continuum PTA60) pumped by a regenerative amplifier (Continuum RGA 60). It delivers a typical output pulse of ≈1 ps duration, centered at 600 nm (16660 cm^{-1}) with an energy of 1.5 mJ at a 10 Hz repetition rate. The second harmonic of this pulse at 300 nm (33330 cm^{-1}) is used as pump pulse. The 600 nm pulse, after passing through an optical delay line (60 fs steps), is focused on a rotating quartz plate to generate a continuum of light which extends from 30000 to 10000 cm^{-1}. This continuum is sent through the sample as the probe beam. Changing the position of the optical delay line allows observation of the transient spectra by use of an optical multichannel analyzer (spectral shape and optical density as a function of time) on a picosecond time scale (sum of excited state absorption (ESA) and gain spectra). The angle between the polarizations of the probe and pump beams were adjusted to 54.7° (the "magic angle") to ensure kinetics free from reorientational effects.

2.3. Correction and Fitting of the Results. ***a. Chirp Correction of the Transient Spectra.*** Because of group velocity dispersion (GVD) and self-phase modulation (SPM), the spectral components of the probe beam do not all reach the sample at the same time. At short delays this effect, known as spectral "chirp", distorts the kinetics and deforms the recorded spectra. Using the optical Kerr effect in pure solvents, we measured this chirp from 10000 to 30000 cm^{-1}. All the spectra presented are corrected for this effect using a homemade algorithm.

b. Fitting and Modeling the Kinetics. Kinetic modeling was based on the assumption that the population of excited molecules

formed in the state directly reached after excitation (the Franck−Condon state) can be transformed into successive excited states until a final state is reached which decays to the ground state. If the number of possible excited states is N then the kinetic scheme can be described as follows:

$$S_0 \xrightarrow{h\nu} S_1 \xrightarrow{k_{12}} S_2 \xrightarrow{k_{2N}} S_N \xrightarrow{k_{N0}} S_0$$

where the S_1, S_i, S_N are the different excited states involved in the transformation process and the k_{ij} are the kinetic constants. Each state S_i has its own characteristic absorption and gain spectrum, with the molar absorption coefficient $\epsilon_i(\nu)$ at wavenumber ν. If at any time t_p the population of the excited state S_i is $P_i(t_p)$, the optical density OD (t_p, ν_n) at time t_p and wavenumber ν_n outside the $S_0 \rightarrow S_n$ absorption spectral range is given by eq 1.

$$OD_{n,p}.\ (t_p, \nu_n) \propto \sum_{i=1}^{i=N} P_i(t_p) \times \epsilon_i(\nu_n) \qquad (1)$$

From the kinetic scheme described above, the populations P_i should follow the differential equation:

$$d/dt \begin{pmatrix} P_1 \\ P_2 \\ P_N \end{pmatrix} = (k_{ij}) \times \begin{pmatrix} P_1 \\ P_2 \\ P_N \end{pmatrix} + \begin{pmatrix} a\, I_{pump}\,(t) \\ 0 \\ 0 \\ 0 \end{pmatrix} \qquad (2)$$

From the measured optical density at different wavenumbers in the spectral range 10000−30000 cm^{-1}, the solution of the system of eq 1 and 2 by the "Runge−Kutta"-algorithm leads to the different kinetic constants k_{ij} and the absorption spectra $\epsilon_i(\nu)$ of the states involved. The limited precision of the measurements enforced the number of states to be determined to a maximum of three (N = 3). In the fitting procedure, the excitation pulse was modeled as a Gaussian shaped pulse the half-width of which was measured by the optical Kerr effect. All fits were performed by neglecting possible back reactions.

2.4. Absorption and Fluorescence Spectroscopy. Technical details about the measurement of absorption and fluorescence spectra, lifetimes and quantum yields are reported elsewhere.[3,4,10]

2.5. Quantum Chemical Calculation of the Transient Spectra. Transition energies (ν), oscillator strengths (f), symmetries (sym), and geometries of the first and second excited singlet states (S_1 and S_2) are obtained using the BFGS geometry optimization algorithm in combination with a complete active space configuration interaction calculation (CAS-CI) including the five highest occupied and five lowest virtual molecular orbitals. Typically 10^5 configurations were generated from which around 100 are finally selected for the CI calculation. Increasing the orbital window up to 18 active MOs (10^8 configurations) does not significantly alter the spectral results. The semiempirical Austin Model 1 (AM1) Hamiltonian contained in the AMPAC 5.0 program was employed on a HP735 workstation.[43] The most characteristical differences of the geometries in S_1 and S_2 are the interannular twist angle (φ) and bond length (r_b) and the dihedral angle between the methyl groups of the dimethylamino substituent and the linked benzene unit (α_N), which is a measure for pyramidalization of the nitrogen. The twist angle of the dimethylamino group is 0° in S_0-S_2. These optimized structural data (S_0 geometries as obtained elsewhere[3,4]) for **I**−**III** are in increasing order:

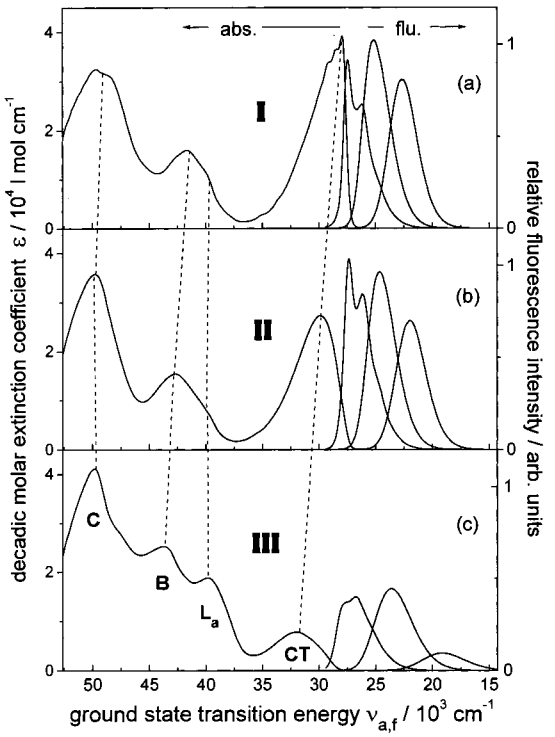

Figure 1. (Parts a−c): steady-state absorption spectra in *n*-hexane and fluorescence spectra in *n*-hexane, diethyl ether, and acetonitrile (from the left to the right) of **I**−**III**.

TABLE 1: Fluorescence Radiative Lifetimes $\tau_r = \tau_f/\Phi_f$ of I−III at Room Temperature in Solvents of Increasing Polarity

solvent	I	II	III
n-hexane (HEX)	2.4 ns	1.7 ns	3.8 ns
diethyl ether (EOE)	2.0 ns	2.1 ns	8.3 ns
triacetine (TAC)	2.4 ns	2.4 ns	10.2 ns[a]
acetonitrile (ACN)	2.6 ns	2.8 ns	36.5 ns

[a] Average lifetime $\langle\tau_f\rangle = (\alpha_1\tau_1 + \alpha_2\tau_2)/(\alpha_1 + \alpha_2)$ of the two long lifetime components at λ_f = 410 nm.

S_0 (1^1A): $\varphi = 0°, 39°, 78°$. $r_b = 1.452, 1.459, 1.467$ Å. $\alpha_N = 18°, 18°, 19°$

S_1(2^1A = ^{1}CT): $\varphi = 0°, 15°, 46°$. $r_b = 1.407, 1.413, 1.427$ Å. $\alpha_N = 2.0°, 1.6°, 1.4°$

S_2(1^1B = ^1L_b): $\varphi = 0°, 32°, 52°$. $r_b = 1.443, 1.459, 1.450$ Å. $\alpha_N = 2.7°, 1.1°, 15°$

3. Results

3.1. Steady-State Spectra and Expectations. The absorption spectra of the biphenyls **I**−**III** have been analyzed in detail elsewhere.[3] Briefly, the four apparent bands denoted as CT, L_a, B, and C in Figure 1 mainly correspond to electronic transitions from the ground state $S_0(1^1A)$ into the terminal states ^{1}CT and ^1L_b (CT band, ^1L_b belongs to the H band in ref 3), ^1L_a (L_a band), ^1B_b (B band) and ^1B_a,^1C_b, and ^1C_a (C band, the ^1C_a-type state is not listed in ref 3) as specified in ref 3. The lowest excited singlet state S_1 of the **I**−**III** investigated is identified as an intramolecular ^{1}CT state transferring charge from the dimethylanilino (donor) to the benzonitrile (acceptor) unit in any relaxed solvent surrounding.[3,4,9,10] The large solvatochromic shift of the fluorescence (Figure 1) confirms the strong electron-transfer character of S_1. It can be assigned to the long-axis-polarized

2^1A state if we consider all three molecules to belong to the same symmetry point group C_2, disregarding the disturbing effect of the fluorene bridging in **I**, with the central biphenyl bond as the symmetry C_2-axis. The short radiative lifetimes determined for **I** and **II** (see Table 1) demonstrate that the lowest singlet transition is of strongly allowed character and corroborates the above assignment for S_1 to the 2^1A state.[3,4] The polarity dependent and long radiative lifetimes for **III** in dipolar solvents have previously been interpreted by an adiabatic photoreaction toward a more decoupled geometry between the dimethylanilino and benzonitrile moiety induced by an increased twist of the interannular bond.[4,9,10]

The fluorescence and absorption results (Figure 1) lead us to predict the following main differences for the transient absorption experiments of the pretwisted biphenyl **III** as compared to the more planar biphenyls **I** and **II**: (1) the stronger solvent stabilization of ^{1}CT in **III** should yield a larger blue shift of the main transient band as compared to **I** and **II**; (2) An additional structural relaxation within the ^{1}CT state should be observed for **III** in polar solvents associated with different spectral features; (3) Similar to the L_a band observed only in the ground-state absorption spectrum of **III**, the decoupling of the ^{1}CT(2^1A) and ^1L_a(3^1A) state in **III** may lead to an additional transient band not visible in **I** and **II**.

3.2. Transient Absorption Measurements. For these studies we used four different aprotic solvents in order to vary the polarity from nonpolar *n*-hexane (HEX) to strongly polar acetonitrile (ACN), together with diethyl ether (EOE) of intermediate polarity. The viscosity of these three solvents is small and practically equivalent associated with comparable solvent relaxation times τ_S (see below Table 3). Triacetine (TAC) was additionally chosen because of its high viscosity at room-temperature associated with intermediate polarity. This solvent should slow the possible processes related to viscosity and allow a better understanding of the photophysical behavior. The time delays 1, 5, and 40 ps are selected for the presented spectra in all fast relaxing solvents (HEX, EOE, ACN). This facilitates the comparison of spectral evolutions in different solvents. As a compromise, the kinetics can readily be followed by the time traces or contour plots. Let us now treat in detail these different experimental conditions.

3.2.1. N-Hexane Solutions. As shown in Figure 2, the behavior of the three compounds in *n*-hexane (HEX) is quite comparable. We mainly observed a broad absorption band around 22000 cm^{-1} (450 nm) and a possible gain band near 26000 cm^{-1} (385 nm) for **I** and **II** and 27000 cm^{-1} for **III** without strong spectral evolution as a function of time. Only a small narrowing of the 22000 cm^{-1} absorption band with time is slightly apparent. In compound **III**, also a weak absorption band near 11800 cm^{-1} (850 nm) appears at later times which is not observed, within experimental error, in compounds **I** and **II** (the positive signal in **I** and **II** at 11000 cm^{-1} is due to second order of diffraction of the 22000 cm^{-1} absorption band). Whether or not the depression appearing in the spectra at 26000−27000 cm^{-1} corresponds to gain is difficult to ascertain, because negative optical density is weak at this energy due to the overlap with the strong absorption. This depression is more pronounced at later times and could be explained by a possible second gain species which is stronger than that of a first species. This would indicate that the transition to the ground state 1^1A of a second species is of more allowed character. From the steady-state and ns time-resolved fluorescence results, the relaxed S_1 state in HEX is indeed located around 27000 cm^{-1} and is highly allowed (τ_r < 3.8 ns).

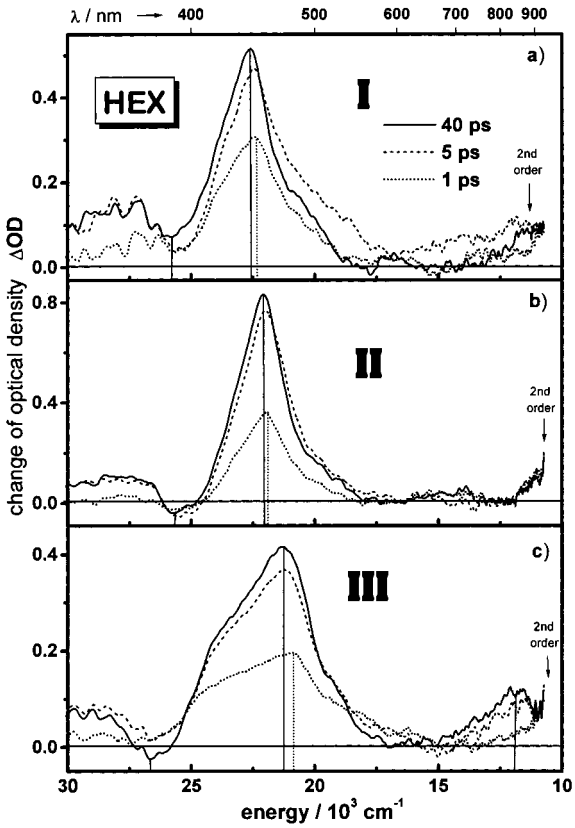

Figure 2. (Parts a−c): transient absorption spectra in *n*-hexane (HEX) for (a) **I**, (b) **II**, and (c) **III** at 1 ps (···), 5 ps (− −), and 40 ps (—) time delays between pump and probe beam. Full vertical lines at maxima and minima indicate the transitions in the relaxed spectra.

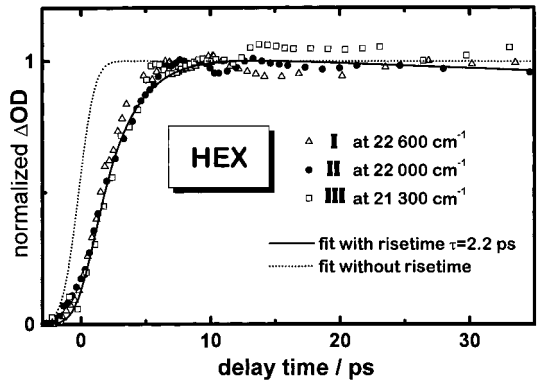

Figure 3. Normalized kinetics for **I**−**III** of the main transient absorption band in *n*-hexane. Simulation curves using a one-state model (···) and a two-state model (—) indicate the existence of two excited-state species, the precursor one being less visible than the successor one.

Typical kinetics at the transient absorption maxima of **I**−**III** are shown in Figure 3. It is not possible to fit these kinetics within experimental error taking into account the presence of a single excited state only, formed during the excitation pulse and decaying on a ns time scale. The rise time observed (2.2 ps) is clearly longer than the limit imposed by the pulse duration as shown in Figure 3. The presence of two excited species is therefore indicated. The initially populated species is denoted as the Franck−Condon species **FC**. (Note, that species are printed in bold in order to be distinguished from electronic states. In this respect, two species can belong to one state, but not vice versa.) In 2.2 ps a second excited species (charge-transfer species **CT**) with stronger absorption signal is formed decaying on a ns time scale (1.2−1.4 ns). But on account of the fact

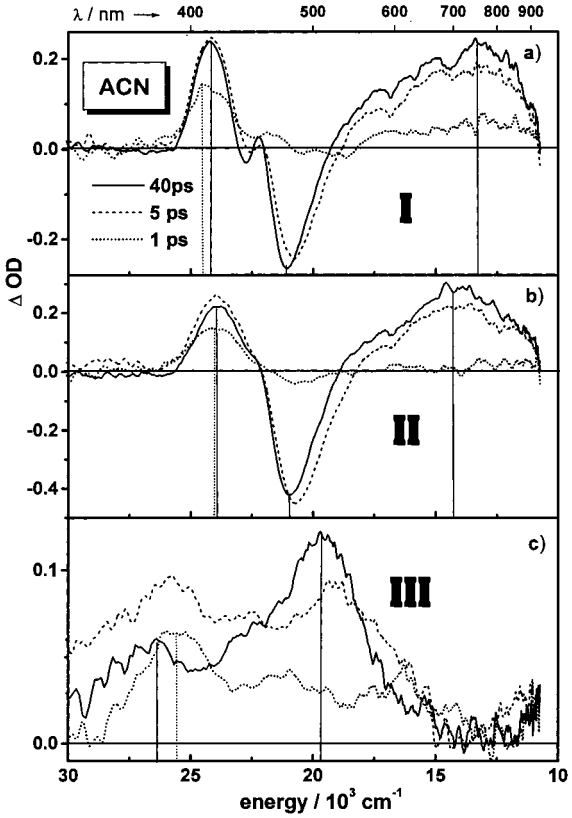

Figure 4. Transient absorption spectra in acetonitrile (ACN) for (a) **I**, (b) **II**, and (c) **III** at 1 ps (···), 5 ps (− −), and 40 ps (—) time delays between pump and probe beam. Full vertical lines at maxima and minima indicate the transitions in the relaxed spectra, and the dotted vertical lines indicate the transitions in the first picoseconds.

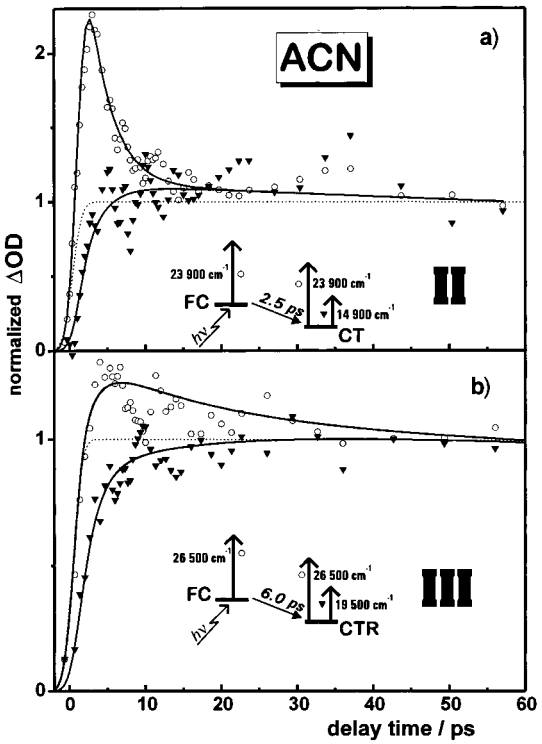

Figure 5. Normalized kinetics for (a) **II** and (b) **III** of the high-energy and the low-energy transient absorption bands in acetonitrile. The continuous lines are the fits obtained using the kinetic model of two states (**FC** and **CT**/**CTR**) shown as an inset. The dotted lines are the fits using a one-state model taking into account the pump pulse profile.

that (only) in this solvent the spectral changes are very weak and a small narrowing is observed, at this point we cannot rule out the alternative explanation of vibrational cooling. Delayed absorption and band narrowing are typical features of such a process and may take place on the ps time scale.[44]

3.2.2. Acetonitrile Solutions. In the very polar solvent ACN with considerable stabilization of the ^{1}CT state (Figure 1), strong evolution of the transient spectra (Figure 4) is observed for **I**−**III** as compared to HEX solutions.

The behavior of compounds **I** and **II** is practically identical in ACN as shown in Figures 4a and b. Following the excitation pulse profile in time, an absorption band appears near 24000 cm^{-1} (425 nm). As time evolves, in contrast to the behavior in HEX, the intensity of this band begins to decrease after two picoseconds (Figure 5a) accompanied by the simultaneous rise of a second absorption transition in the red part of the spectrum near 13−14000 cm^{-1} and a broad gain band at 21000 cm^{-1} (475 nm). The energy and strong intensity of the gain band in **I** and **II** (Figure 4a,b) is consistent with the static fluorescence maximum (Figure 1) and the large radiative rates (Table 1) for the ^{1}CT state of **I** and **II**. Due to the obvious charge-transfer properties of the successor species, it is termed as **CT**, whereas the less solvent stabilized precursor species is related to **FC** as above.

The kinetics at energies corresponding to the high-energy and low-energy absorption bands, respectively, are identical for **I** and **II** and are therefore shown in Figure 5a, only for **II**. They can obviously be rationalized by a precursor−sater relationship between the initially excited species **FC** only associated with the high-energy absorption band and the product excited species **CT** characterized by the gain band (21000 cm^{-1}) and the broad absorption at 14000 cm^{-1}. The **CT** species is formed from **FC** with a rate constant of (2.5 ps)$^{-1}$ and decays on a nanosecond time scale (Figure 5a). A contribution from the **CT** species to the absorption around 24000 cm^{-1} has to be considered because the signal does not vanish after 2.5 ps.

The behavior of **III** is completely different from that of compound **I** and **II** in this solvent (Figures 4c and 5b). First of all, a gain band is absent for **III** in ACN which reflects the long radiative lifetimes of the S_1 state as compared to **I** and **II**. The excitation process is followed by the appearance of a weak absorption at 25600 cm^{-1} (390 nm) part of which decays with an approximate time constant of 6 ps. This transient band is strongly shifted to the higher energy region with respect to the corresponding bands of **I** and **II** indicating the relaxation from **FC** to a charge-transfer species (denoted as **CTR** in Figure 5b instead of **CT** in Figure 5a) which is more relaxed than in **I** and **II**. A second and more intense absorption band near 19500 cm^{-1} (515 nm) appears with the same time constant as the high energy band decreases demonstrating their mother−daughter relation. The decay to the ground state occurs on a nanosecond time scale (7.6 ns).

The spectral behavior and existence of two species is well illustrated on the contour-map of **II** in ACN (Figure 6). Here, black color signifies positive absorption and white color negative absorption or gain, respectively. The first species, the Franck−Condon excited species **FC**, is represented by one absorption region (**ESA$_{FC}$**) around 24000 cm^{-1}. With increasing time, part of this absorption decays quickly and a gain "valley" (**g$_{CT}$**) appears. Its temporal maximum exactly coincides with the low-energy absorption "mountain" (**esa$_{CT}$**). There, the maximum population of the **CT** species is reached.

3.2.3. Diethyl Ether Solutions. In this solvent (EOE) of intermediate polarity between HEX and ACN, we expected intermediate behavior. Because of almost equal features of **I**

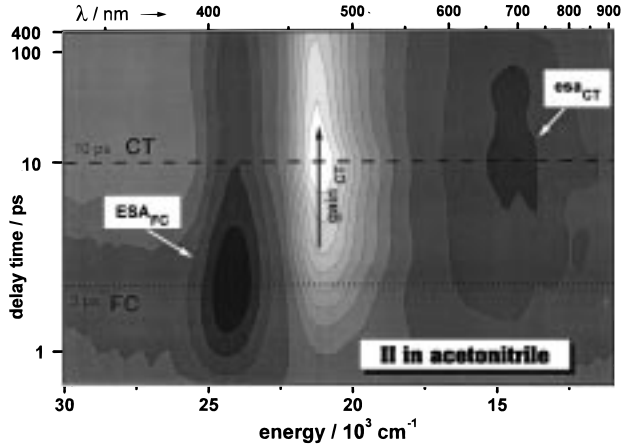

Figure 6. Contour plot of the transient absorption spectra of **II** in acetonitrile in the energy range of 30000−11000 cm^{-1} and in the delay time range of 0−400 ps. Broken lines indicate the time delays when the spectral characteristics of the **FC** and **CT** species, respectively, are best revealed.

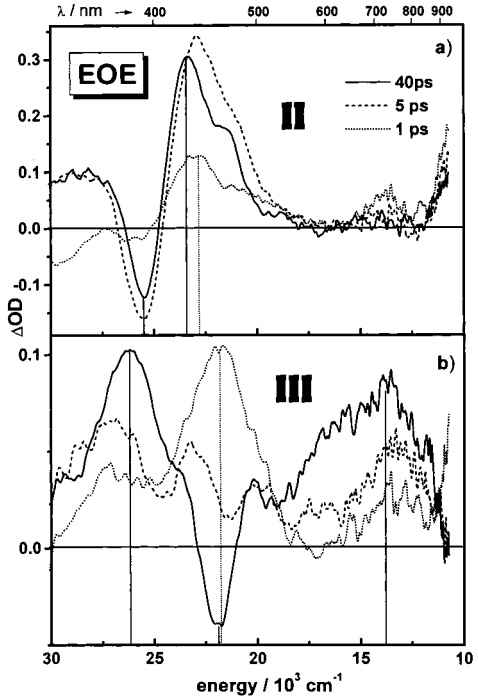

Figure 7. Transient absorption spectra in diethyl ether (EOE) for (a) **II** and (b) **III** at 1 ps (···), 5 ps (− − −), and 40 ps (—) time delays between pump and probe beam. Full lines at maxima and minima indicate the transitions in the relaxed spectra, and the dotted lines indicate the transitions in the first picoseconds of the Franck−Condon species (**FC**).

and **II** in HEX and ACN as well as in TAC (see section 3.2.4), we did not investigate **I** in EOE supposing identical behavior in this solvent, too. The spectral shapes of compound **II** are practically the same as in HEX (see Figure 7a) with the transitions at similar energies. However, the assignment of the depression observed at 26000 cm^{-1} (385 nm) in HEX (Figure 2b) to a gain band is more clearly demonstrated by the strong negative signal in EOE after 4 ps (Figure 7a). Furthermore, a significant temporal evolution of the band shape is observed: the absorption band near 23000 cm^{-1} (435 nm) narrows, shifts to the blue with a long wavelength shoulder similar but more pronounced than that in HEX, and at the same time the gain band slghtly shifts to the red.

Typical kinetics for **II** at an energy where the contribution

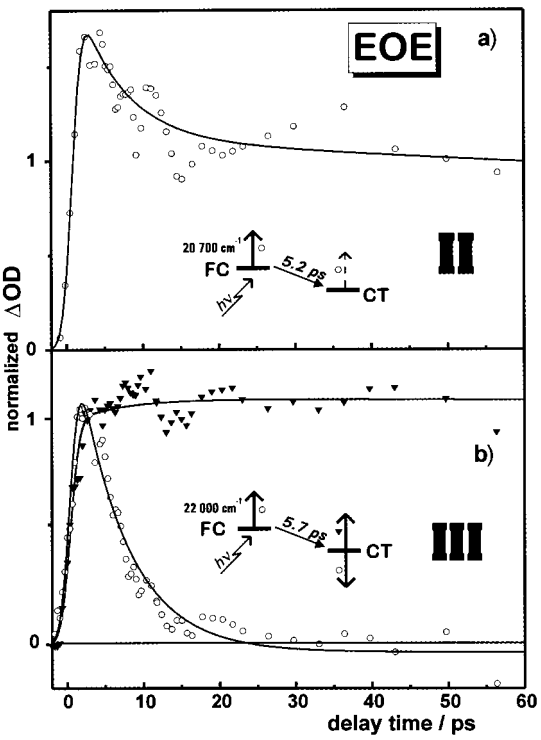

Figure 8. (a): Normalized kinetics of the transient absorption band at 20700 cm^{-1} for **II** in diethyl ether. (b): Normalized kinetics of the rise of the high energy absorption for **III** at 26200 cm^{-1} and the transformation of the Franck−Condon absorption band into the gain band at 22 000 cm^{-1}. For a and b, the applied kinetic Schemes of two states (**FC** and **CT**) and the related simulation curves are also shown.

of the **FC** species is relatively high are shown in Figure 8a. The fit (τ = 5.2 ps) is based on a precursor (**FC**)−successor (**CT**) model with the spectral characteristics of both species being rather similar.

For compound **III** (Figure 7b), the spectral changes are more evident. Just after excitation two maxima appear: one weak maximum near 28000 cm^{-1} and a stronger one near 21900 cm^{-1}. A minimum appears at about of 25000 cm^{-1}, between these two maxima. From comparison to the HEX spectra we can assign this minimum to a weak gain band of the **FC** species which is overlapped with a strong absorption band. As time evolves, the maximum at 21900 cm^{-1} transforms into a gain band with considerable negative optical density. At intermediate time delays (5 ps), the spectrum exhibits dual fluorescence gain of **FC** and **CT** (Figure 7). In the red part of the spectrum, a weak absorption band exists around 13800 cm^{-1} (750 nm), the kinetics of which could not be extracted due to a low signal-to-noise ratio. Within the first 40 ps, the kinetic behavior of **III** can be described by the same model as above using a time constant of 5.7 ps (Figure 8b). However, a blue shift of the low-energy absorption may indicate a further relaxation process.

3.2.4. Triacetine Solutions. In this solvent (TAC) of intermediate polarity but high viscosity, we expected a similar spectral behavior as in EOE for all compounds. On the other hand, the slow solvation process should lengthen the observation time of the primary excited **FC** species.

In Figure 9, typical transient spectra are shown for **I**−**III** in TAC. They are similar concerning the spectral shapes, but differ in time evolution, energy position, and relative absorbance. All spectra of the initially populated species **FC** (3 ps) possess a strong absorption band (23000−24000 cm^{-1} for **I** and **II**, 25000 cm^{-1} for **III**) modulated in **I** and **II** by a fluorescence gain band at 25400 cm^{-1} not far from the position of the gain (25500 and

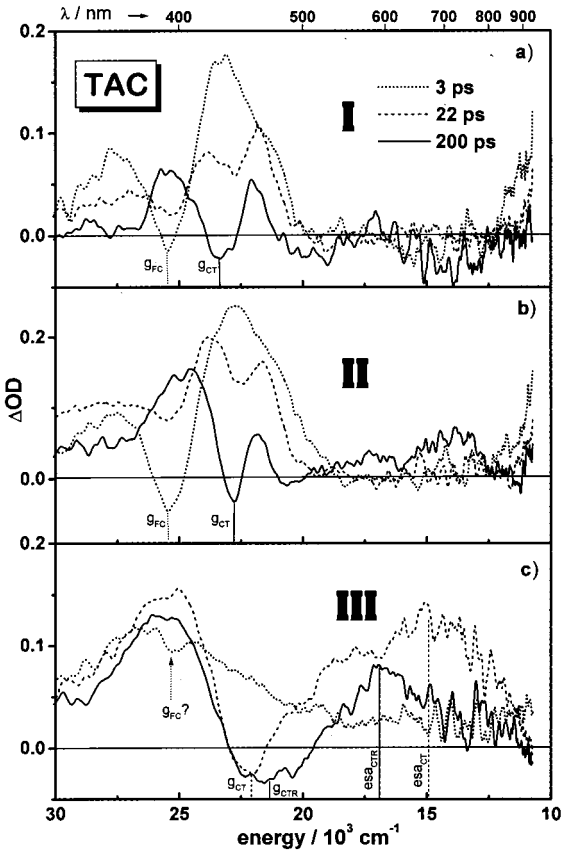

Figure 9. Transient absorption spectra in triacetine (TAC) for (a) **I**, (b) **II**, and (c) **III** at 3 ps (···), 22 ps (− − −), and 200 ps (—) time delays between pump and probe beam. For **I** and **II**, dotted and full vertical lines at minima indicate the positions of the Franck−Condon ($\mathbf{g_{FC}}$) and charge-transfer gain bands ($\mathbf{g_{CT}}$). For **III**, the Franck−Condon gain is less developed (depression at 25000 cm^{-1}). Broken and full vertical lines for **III** indicate the gain and low-energy transient absorption bands for the **CT** species and the more relaxed **CTR** species, respectively.

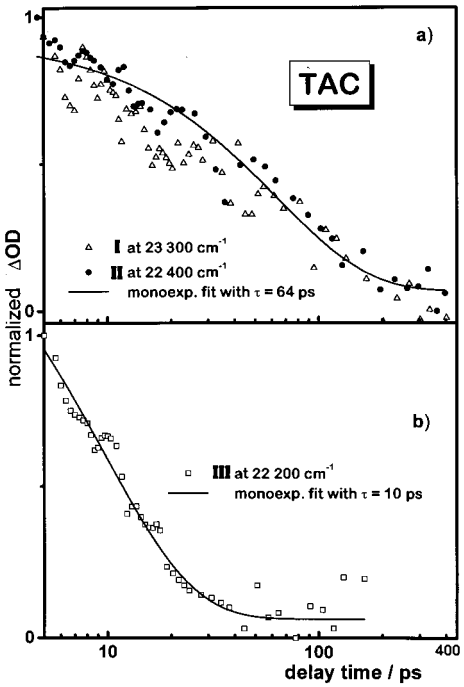

Figure 10. Normalized kinetics for **I**−**III** in triacetine of the transformation from the transient absorption bands of the **FC** species into the gain bands of the **CT** species plotted on a logarithmic time scale. Monoexponential decay simulation curves are plotted for **II** and **III**. The corresponding lifetimes are 69(±20) ps for **I**, 64(±15) ps for **II**, and 10(±2) ps for **III**.

25900 cm^{-1}) and steady-state fluorescence band (26900 and 26600 cm^{-1}) in HEX. Let us term this strong absorption band $\mathbf{ESA_{FC}}$ and the corresponding gain band $\mathbf{g_{FC}}$. In **III**, only a depression in the $\mathbf{ESA_{FC}}$ band is apparent at 25000 cm^{-1}, but it is too weak for a firm assignment to a gain band. Thus we have to note that, comparing **III** with **I** and **II**, the gain $\mathbf{g_{FC}}$ is much stronger that in **I** and **II**. At this short time delay, there is no indication for a low-energy absorption band neither for **I** and **II** nor for **III**. With a proceeding time delay, $\mathbf{g_{FC}}$ weakens and a new fluorescence gain appears for all compounds at 23400 cm^{-1} (427 nm) in **I**, 23000 cm^{-1} (435 nm) in **II**, and 22100 cm^{-1} (452 nm) in **III** which we assign to the gain $\mathbf{g_{CT}}$ of the charge-transfer species. It is very important to stress that there is no gradual shift with time of the initial gain bands from around 25400 cm^{-1} ($\mathbf{g_{FC}}$) to the position of the band $\mathbf{g_{CT}}$, but a weakening of the gain $\mathbf{g_{FC}}$ accompanied by a growing of the $\mathbf{g_{CT}}$ gain. This means that all donor−acceptor biphenyls studied show dual fluorescence (here observed as dual gain) with precursor−sater relationship within a few picoseconds. The second gain band $\mathbf{g_{CT}}$ of **I** and **II** establishes exactly at the location of the steady-state emission at 23600 cm^{-1} (424 nm) for **I** and 23000 cm^{-1} (434 nm) for **II**. In contrast to **I** and **II**, the center of the gain $\mathbf{g_{CT}}$ in **III** after 22ps at 22100 cm^{-1} (452 nm) does not coincide exactly with the steady-state emission maximum at 20700 cm^{-1} (484 nm). But on a longer time scale (200 ps), the gain band $\mathbf{g_{CT}}$ of **III** broadens to the red and then its center coincides with the steady-state emission maximum. The broadening of the gain band in **III** for longer times is not the only difference to **I** and **II**. **III** also exhibits an additional weak low-energy absorption band around 15000−17000 cm^{-1} which can be assigned to the transition $\mathbf{esa_{CT}}$, not seen in **I** and **II**. Similar to the behavior in diethyl ether, this band seems to blue shift with time, accompanied by the broadening of the gain $\mathbf{g_{CT}}$. In Figure 10, the kinetics at the energies of the gain bands $\mathbf{g_{CT}}$ for **I**−**III** are shown. To illustrate the confidence of the fits and to compare the different time scales of the kinetics in **I** and **II** with **III**, the time axis is on a logarithmic scale. For **I** and **II**, the kinetics of the **CT** formation are quite comparable (69 ps for **I** and 64 ps for **II**), but are clearly slower than for **III** (10ps).

The time evolution of the spectra can vividly be followed on the contour maps of **II** and **III** in Figure 11. For **II**, the maximum population of the **FC** species is characterized by a strong absorption region ($\mathbf{ESA_{FC}}$) and a gain valley ($\mathbf{g_{FC}}$) at short time delays, whereas for **III** only an absorption mountain of **FC** is well pronounced. The appearance of the gain valley ($\mathbf{g_{CT}}$) at longer time delays indicates the population of the **CT** species in both maps. In accord with the gain time traces in Figure 10, the gain valley of **CT** (i.e., maximum population of **CT**) is deepest at delay time 200 ps for **II** but already at 40 ps for **III**. The gain $\mathbf{g_{CT}}$ of the flexible biphenyl **II** exhibits a slight anomalous blue shift with increasing time which might be due to an overlapping red shifted absorption band of the **CT** species. However, the gain in **III** clearly broadens with time to the low-energy side indicating an additional relaxation to a more relaxed species **CTR** observable only in **III**.

4. Discussion

The discussion is divided into three main parts. In the first part, the observed transient transitions are assigned to electronic states and their polarity and twist angle dependence is inter-

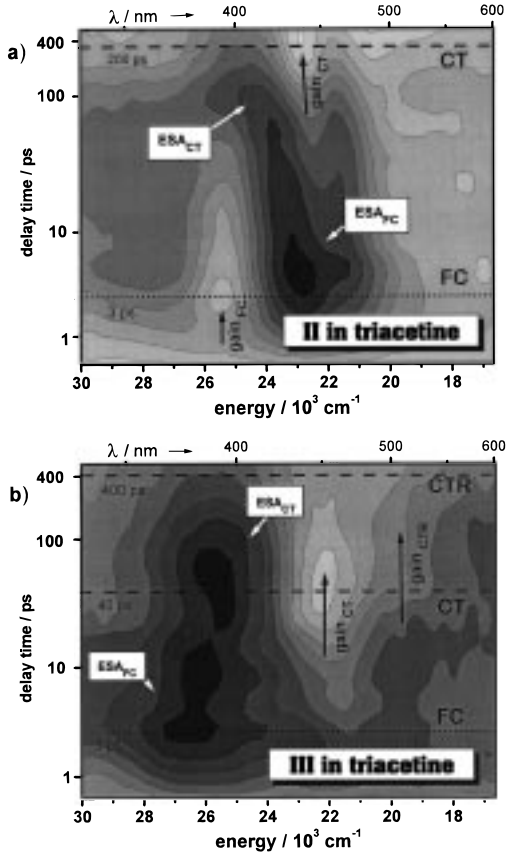

Figure 11. Contourplots of the transient absorption spectra of (a) **II** and (b) **III** in triacetine in the energy range of 30000−16000 cm^{-1} and in the delay time range of a nonlinear time scale from 0 to 450 ps. Broken lines indicate the time delays when the spectral characteristics of the **FC**, **CT**, and **CTR** species, respectively, are best revealed.

preted. In the second section, evidences for structural relaxations are revealed, and the last discussion section deals with the dependence of the charge-transfer rates on solvent and molecular structure.

4.1. Assignments of the Excited-State Absorption and Gain bands and Their Dependence on Polarity and Twist Angle. Five bands can be correlated for all compounds: two gain bands, one of the precursur species **FC** ($\mathbf{g_{FC}}$) and the other of the successor species **CT** or **CTR** ($\mathbf{g_{CT}}$ or $\mathbf{g_{CTR}}$), and three transient absorption bands, the first one belonging to **FC** ($\mathbf{ESA_{FC}}$) and the next two high- and low-energy successor bands associated with the **CT** or **CTR** species ($\mathbf{ESA_{CT/CTR}}$) and $\mathbf{esa_{CT/CTR}}$). The transient transitions from the **CT** and **CTR** species undoubtedly originate from the $^1CT(2^1A)$ state as evidenced by the solvatochromism of the gain bands. But the origin of the **FC** species is under discussion.

4.1.1. Assignments of the Absorbing and Emitting Species to Two States. In a first approximation, the experimental energy (ν_{exp}) of the excited-state absorption $S_x \rightarrow S_n$ should resemble the difference ($\Delta\nu_{ss}$) of the photon energy for the ground-state absorption $S_0 \rightarrow S_n$ and the emission $S_0 \leftarrow S_x$ process. Comparing the $\mathbf{ESA_{FC}}$ and $\mathbf{ESA_{CT}}$ transition energies in HEX ($\nu_{exp} = 21-22000$ cm^{-1}) with the energy differences between the absorption (Figure 1) and gain bands ($\Delta\nu_{ss} = \nu_{abs}(S_0 \rightarrow S_n) - g_{FC/CT}$), a good correlation is only found for transitions into the C band ($\Delta\nu_{ss} \approx 23000$ cm^{-1}), because the alternative assignment of transitions into the B band ($\Delta\nu_{ss} \approx 16000$ cm^{-1}) is connected with a too low energy difference. The additional comparison with the quantum chemical (AM1/CI) calculations of the $S_1(^1CT) \rightarrow S_n$, as well as $S_2(^1L_b) \rightarrow S_n$ transitions, presented in Table 2, proves this assignment. In perfect agreement with experiment, the four ground-state absorptions[3] $S_0 \rightarrow {}^1B_b$ (B band) and $S_0 \rightarrow {}^1B_a, {}^1C_a, {}^1C_b$ (C band) are calculated to be very intense ($f_{calc} \geq 0.20$; not shown), whereas from the excited states only the transitions $S_1(^1CT) \rightarrow {}^1C_a$ and $S_2(^1L_b) \rightarrow {}^1C_b$ carry large oscillator strengths ($f_{calc}({}^1C_a, {}^1C_b) \geq 10 f_{calc}({}^1B_a, {}^1B_b)$) and have suitable energy to account for the $\mathbf{ESA_{CT}}$ and $\mathbf{ESA_{FC}}$ bands. Furthermore, the energy of the $\mathbf{esa_{CT}}$ band ($\nu_{exp} \approx 12000$ cm^{-1}) likewise is in nice agreement with both the energy difference between the gain $\mathbf{g_{CT}}$ and the L_a absorption band ($\Delta\nu_{ss} \approx 13000$ cm^{-1}) and, on the other hand, with the calculated transition energy for the $S_1(^1CT) \rightarrow {}^1L_a$ transition (Table 2). Up to $\nu_{calc} = 30000$ cm^{-1}, only long-axis polarized excited-state transitions (symmetry transitions $^1A \rightarrow {}^1A$, $^1B \rightarrow {}^1B$ within C_2 point group) are found to be intense (cf. f_{calc} of $^1B \rightarrow {}^1A$ or $^1A \rightarrow {}^1B$ transitions are less than 0.03), which is exemplified in Table 2 by the low oscillator strength of the $S_0 \leftarrow S_2(^1L_b)$ emission transition. Hence, the short-axis polarization of the $S_2(^1L_b) \rightarrow {}^1L_a$ and the absence of another low-energy S_n state with ^1B symmetry explains that a low-energy transition is not found for the S_2 state, which in turn parallels the absence of a low-energy band $\mathbf{esa_{FC}}$ for the experimental precursor species **FC** in any solvent. It seems therefore very probable that the **FC** species is associated with the calculated $S_2(^1L_b)$ state. Two further correlations from Table 2 confirm this tentative assignment: (i) the calculated oscillator strengths for the proposed precursor state $S_2(^1FC/^1L_b)$ are less than those of the final $S_1(^1CT)$ state explaining that the kinetics of the main transient absorption band (Figure 3) are observed as rise times due to a transformation from a less allowed $S_2(^1FC)$ state to a more allowed $S_1(^1CT)$ state, and (ii) the slight blue shift of the main absorption band with time (Figure 2) is reproduced by the calculated higher energy of the final $\mathbf{ESA_{CT}}$ than of the $\mathbf{ESA_{FC}}$ band.

4.1.2. Effects of Solvent Polarity and Twist Angle. To obtain the experimental transition energies of the excited-state absorption and gain bands, the individual spectra of **FC**, **CT**, and/or **CTR** were extracted and deconvoluted into the absorption

TABLE 2: Assignments of Experimentally Observed Transient Bands (in *n*-Hexane) to Calculated $S_1(^1CT) \rightarrow S_n$ and $S_2(^1L_b) \rightarrow S_n$ Transitions. The Calculated Twist Angles φ of I−III in S_1/S_2 are 0°/0°, 15°/32°, and 46°/52°

	ν_{exp} [10^3 cm^{-1}]			ν_{calc} [10^3 cm^{-1}]			f_{calc}[a]				
band I−III	I	II	III	I	II	III	I	II	III	transition **I−III**	sym **I−III**
ESA_{FC}	22.5	21.9	20.9	24.0	22.4	20.2	0.28	0.28	0.22	$^1L_b \rightarrow {}^1C_b$	$^1B \rightarrow {}^1B$
ESA_{CT}	22.7	22.1	21.4	23.3	24.7	23.4	1.02	1.26	0.43	$^1CT \rightarrow {}^1C_a$	$^1A \rightarrow {}^1A$
esa_{CT}			11.8	7.8[b]	8.7[b]	10.3[b]	0.07[b]	0.11[b]	0.19[b]	$^1CT \rightarrow {}^1L_a$	$^1A \rightarrow {}^1A$
g_{FC}	−25.9[c]	−26.1[c]	−26.6[c]	−29.1	−32.0	−30.6	−0.02	−0.03	−0.02	$^1L_b \rightarrow S_0$	$^1B \rightarrow {}^1A$
g_{CT}	−25.9	−26.1	−26.6	−25.6	−27.2	−28.7	−0.57	−0.76	−0.58	$^1CT \rightarrow S_0$	$^1A \rightarrow {}^1A$

[a] The oscillator strength of all other calculated transitions up to 35000 cm^{-1} are less than 0.05 (except the $S_1(^1CT) \rightarrow {}^1B_a$ transition of **I** and **II** with $\nu_{calc} \approx 19000$ cm^{-1} and $f_{calc} = 0.15$. cf. **III**: $\nu_{calc} = 17000$ cm^{-1} and $f_{calc} = 0.03$). [b] Due to strong coupling between the close lying ^1L_a states 3^1A and 4^1A (see ref 3), ν_{calc} corresponds to the more intense ^1L_a transition and the sum of both oscillator strength (less geometry dependent than single values) is given as f_{calc}. [c] Position of dips in early spectra.

SCHEME 2: Energy Level Diagram of II and III in *n*-Hexane, Diethyl Ether and Acetonitrile (HEX, EOE, and ACN) as Derived from the Transient Absorption Spectra[a]

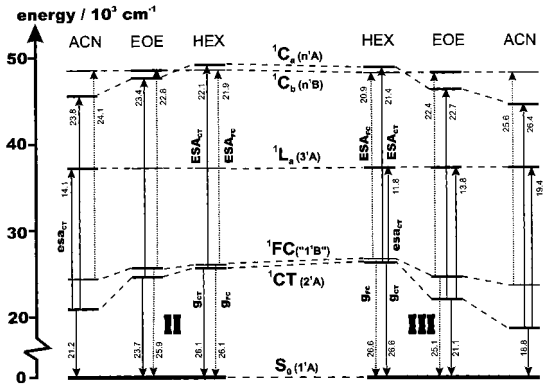

[a] The energy of the ground state has been taken as zero. The energy levels of which the absolute energetical position could not be determined directly by the experiments are drawn with thinner lines. Transitions from the ^{1}FC state 1^1B (**ESA$_{FC}$** and **g$_{FC}$**) are indicated by dotted arrows and the transitions from the ^{1}CT state 2^1A (**ESA$_{CT}$**, **esa$_{CT}$**, and **g$_{CT}$**) by full arrows.

and gain contributions using Gaussian functions. The energetical positions of the lower states or species, respectively, relative to the ground state can be derived from the gain positions. In such cases where gain is not observed (e.g., for **FC** in ACN) the energy is extrapolated taking into account the solvatochromic shift of the observable gain bands. Using all these information, the solvent dependent transitions are plotted in an energy diagram (Scheme 2).

Gain bands. Gain bands (**g$_{FC}$** and **g$_{CT}$**) are produced by stimulated emission due to the probe beam. It has been shown[45] for organic dyes that gain is absent for radiative lifetimes longer than 10 ns, this property being inversely related to the fluorescence transition dipole moment M_f which controls the stimulated emission efficiency. Accordingly, gain of the ^{1}CT state is observed in all cases except for **III** in ACN, which has a radiative lifetime of more than 30 ns (Table 1) connected with a comparatively small M_f value (2.3 D).[4,9] On the other hand, the negative optical density (ΔOD) of the gain band **g$_{CT}$** of **I** and **II** increases relative to the positive ΔOD of the **ESA$_{CT}$** band with solvent polarity leading to a very intense gain band in ACN (Figure 4). This is consistent with our previous observation that the transition dipole moment M_f of the $S_0(1^1A)$←$S_1(^1CT)$ fluorescence increases with polarity in **I** and **II**[4,9] and, moreover, with the observation of Lahmani et al.[2] that the picosecond time decay of the integrated fluorescence intensity is not as fast as it would have been expected, if the solvation reduces M_f of the ^{1}CT emission. It can therefore be supposed that the electronic interaction of $S_1(^1CT)$ with the less allowed $S_2(^1L_b)$ state decreases with solvent polarity due to an inreasing S_1-S_2 energy gap (ΔE^1_{CT-1Lb}). Furthermore, gain should be located at energies matching the steady state fluorescence maxima. In fact, the gain bands observed in HEX agree with the fluorescence maxima. However, only the gain **g$_{CT}$** exhibits a solvatochromism similar to the steady-state fluorescence (Figure 1) confirming that the state responsible for **g$_{CT}$** is the ^{1}CT state.[1,4,9,10] Nevertheless, the slight red shift of the gain **g$_{FC}$** with increasing polarity reveals a nonnegligible ET character of the **FC** species, too.

ESA Bands. The two ESA bands observed previously in 9,9′-bianthryl (BA) were assigned to a locally excited (^{1}LE) and ^{1}CT state.[7,11,12] The insensitivity of the $^1CT\rightarrow S_n$ transition energy on solvent polarity has been explained by a similar, near complete ET character in the lower and upper state. In contrast to BA, an increase of the energy for the **ESA$_{CT}$** and **esa$_{CT}$** bands with increasing solvent polarity is observed for **I**−**III** due to transitions from the strongly stabilized ^{1}CT state into the upper states ^1C_a and ^1L_a with smaller ET character. As expected from the larger dipole moment of the ^{1}CT state for **III** in comparison to the moments of the states for **I** and **II**,[4] the increase of transition energy of **ESA$_{CT}$** with polarity is strongest for **III**. We also note in Scheme 2 that even the **ESA$_{FC}$** bands are blue shifted with increasing solvent polarity. In accord with the solvatochromism of the gain bands **g$_{FC}$**, this supports that the **FC** species possesses significant ET character, too. Regarding the twist angle effect in the case of weak solvent stabilization (HEX and EOE), the comparison of **I** and **II** with **III** reveals that the experimental as well as the calculated **ESA** transitions of the more twisted **III** are redshifted and less allowed as compared to those of the planar **I** and quasi planar **II**. The agreement between the experiments and calculations gives further confidence to the calculation results in Table 2. Needless to say that in the highly polar solvent ACN, the stronger stabilization of the ^{1}CT state for **III** yields a higher **ESA$_{CT}$** transition energy than the energies for **I** and **II**.

esa$_{CT}$ Bands. The **esa$_{CT}$** band is observed in nonpolar to medium polar solvents only for the highly pretwisted compound **III**. This reflects the observation of a maximum for the ground-state absorption $S_0(1^1A)\rightarrow{}^1L_a(3^1A)$ only for **III**. Both long-axis-polarized transitions to the 3^1A state, either from 1^1A or 2^1A, get more allowed with increasing twist angle φ as supported by the calculated oscillator strength of **esa$_{CT}$** in Table 2. As discussed in section 4.2, the average twist angle $\langle\varphi\rangle$ of **III** increases with solvent polarity, which may also explain the increasing intensity ratio ΔOD(**esa$_{CT}$**)/ΔOD(**ESA$_{CT}$**) from HEX to ACN. In polar ACN, however, **I** and **II** also exhibit the **esa$_{CT}$** band. One possibility is that the strong increase of the energy gap between the $^1CT(2^1A)$ and the $^1L_a(3^1A)$ state (ΔE_{La-CT} increase of 5000 cm^{-1} for **II** in ACN as compared to **II** in HEX) leads to a decoupling of these states, similar to the twist effect in **III**. Both decoupling effects (i.e., twisting of the benzene units and increased energy gap may enhance the intensity of the transient $^1CT(2^1A)\rightarrow{}^1L_a(3^1A)$ relative to the $^1CT(2^1A)\rightarrow{}^1C_a(n^1A)$ transition). On the other hand, the **esa$_{CT}$** band of the planar **I** and **II** is located at lower energy than that of **III** in the solvent interaction case (Figure 4) and gas-phase case (ν_{calc} in Table 2). We can therefore not exclude the alternative possibility that the **esa$_{CT}$** band is simply concealed in the energy region (<11000 cm^{-1}) where the detection sensitivity is too low. In any case, experiment and calculations agree that the intensity ratio ΔOD(**esa$_{CT}$**)/ΔOD(**ESA$_{CT}$**) is largest for the twisted **III**.

Mixed Nature of ^{1}FC. The difference in the transition energies between the **FC** and **CT/CTR** species, especially of the gain bands (same final S_0 state) in combination with the precursor−successor relationship of their occurrence, the separate time scales in TAC and the additional low energy band **esa$_{CT}$** only for the ^{1}CT state leads to the conclusion that, beside the ^{1}CT state, the **FC** species can be treated as a second excited state. Moreover, the appearance of the gain **g$_{FC}$** seems to necessitate a low-energy gap to the highly allowed $^1CT(2^1A)\rightarrow{}S_0(1^1A)$ transition **g$_{CT}$** indicating that the $^1FC\rightarrow S_0$ transition needs a vibronic coupling mechanism which in turn points to a different symmetry (^{1}B in C_2 point group) of the zeroth-order ^{1}FC state. These observations suggest that the ^{1}FC state is of substantial ^1L_b character mixed with the ^1L_a-type ^{1}CT state.

Thus, the excited-state electron transfer in the investigated donor−acceptor biphenyls is accompanied with more spectral features than in the extensively studied biaryls 9,9′-bianthryl (BA)[7,11,12,] or 4-(9-anthryl)-*N*,*N*-dimethylaniline (ADMA)[15] and derivatives as well as in the recently studied 9-dimethylanilinophenanthrene (9DPhen) biaryl compounds.[13,14] For BA in triacetine, the ^{1}LE and ^{1}CT transient absorption bands could be separated,[12] but in ADMA,[15] 9DPhen,[13] and related molecules, the time-resolved transient absorption spectra exhibit only a gradual shift with increasing time delay but not such clear spectral differences between the species before and after the electron-transfer step as it is shown for **I**−**III**.

4.2. Structural Relaxation. In a previous fluorescence analysis it was concluded that ^{1}CT emission occurs from planar conformers of **II**, whereas the average twist angle $\langle\varphi\rangle$ in the ^{1}CT state of **III** increases with solvent polarity.[4,10] Because the twist angles in ^{1}CT are different to the ground state, photoinduced structural relaxations of **II** and **III** take place which are investigated in this section.

Independent of the solvent, the flexible biphenyl compound **II** shows rather the same spectral and kinetic excited state behavior (fluorescence and transient absorption) like the planar model compound **I**. These results demonstrate that **II** performs a photoinduced relaxation toward planarity. For the pretwisted biphenyl **III**, similar behavior is observed in HEX. Thus, in agreement with the fluorescence studies, the **CT** species of **II** and **III** can be attributed to a more planar structure than in the ground state.

In the medium polar solvent EOE, the spectrum of the primary precursor species **FC** for **III** (1 ps in Figure 7b) is quite similar to the one observed in HEX solvent (cf. Figure 2c) and the spectrum of the successor species **CT** (40 ps in Figure 7, part b), formed in 5.7 ps, is similar, while slightly shifted to the blue, to the spectrum observed for compounds **I** and **II** in ACN (see Figure 4a and 4b). It seems then that compound **III** in this solvent of intermediate polarity exhibits a behavior which starts, just after excitation, with the HEX situation and evolves to the situation observed in compound **II** and **I** in ACN for longer times. This indicates that in EOE the primary structural relaxation for **III** is the same as that for **II**, namely, to the more planar species **CT**. Hence for **II** and **III**, the **FC** species feeds the ^{1}CT state with a structure more planar than in the ground state. This also agrees with the observation that the relaxation times of **II** and **III** are similar in EOE (5−6 ps) but significantly different in ACN, where a different species **CTR** is populated (see below).

Using time-resolved fluorescence on a nanosecond time scale, an equilibrium between the initially populated more planar species **CT** and a more relaxed (conformationally and by solvent interaction) charge-transfer species **CTR** has been deduced for **III** in EOE.[4,9] Quantum chemical calculations supported the idea of a double minimum twist potential in the ^{1}CT state of **III** in EOE.[4,9,10] Searching for this additional slow relaxation in the transient spectra of **III** in the medium polar solvents EOE and TAC, we can note that (i) the low-energy absorption band $\mathbf{esa_{CT}}$ in EOE (near 13800 cm^{-1} in Figure 7b) reveals a slight blue shift from 5 to 40 ps and (ii) the $\mathbf{esa_{CT}}$ band in TAC shifts to the blue with time, accompanied by a clear broadening of the gain $\mathbf{g_{CT}}$ (Figures 9c or 11b). These transient absorption results may also point to this later relaxation process from **CT** to **CTR**.

In analogy to the fluorescence results,[4,9] the **CTR** species should prevail for **III** in ACN. The observations (Figures 4 and 5) that (i) the kinetics of **III** (6 ps) in ACN are distinctly slower than for **I** and **II** (2.5 ps), (ii) the absorption strongly shifts to the blue, and (iii) that a gain band is absent, are indeed indications that a more stabilized charge-transfer species **CTR** is populated in **III** than in **I** and **II** in ACN. In agreement with our fluorescence results, the more relaxed **CTR** species can then be characterized by a larger dipole moment and a strongly reduced fluorescence transition moment (M_f) as compared to the **CT** species.[4,9] Such properties of the ^{1}CT state are conceivable with a twisted structure of **CTR**. In this case, the transient spectrum of **CTR** should resemble a superposition of the dimethylaniline cation (DMA^+) and benzonitrile anion (BN^-) spectra.

DMA^+ and BN^- ion spectra are characterized by $S_1 \rightarrow S_n$ absorption bands at 21300 cm^{-1} (470 nm)[46,47] and 24700 cm^{-1} (405 nm)[46,48] and both do not possess a gain contribution. The compounds **I** and **II** in ACN, however, show quite different spectra (Figure 4a and 4b) as compared to the sum of DMA^+ and BN^- spectra.[46−48] This supports the idea of the strongly delocalized character of ^{1}CT in **I** and **II** connected with a planar structure. For **III** in ACN (Figure 4c), the low-energy band $\mathbf{esa_{CT}}$ is blue shifted (in comparison to less polar solvents) nearly to the energy that matches the DMA cation band and the high-energy band $\mathbf{ESA_{CT}}$ is close to the transient absorption of the BN anion. The close relation to DMA^+ and BN^- indicates a nearly complete ET similar to BA and is therefore indeed understandable by the photoinduced strongly twisted structure of **III** in ACN as opposed to that of **III** in less polar solvents as well as compared to the structures **I** and **II** in any solvent.

The photoinduced electronic and structural relaxation processes discussed above are summarized in Scheme 3. The rate determining step of the transition from the Franck−Condon region (^{1}FC) to the ^{1}CT state can be attributed to the ^{1}FC→^{1}CT interconversion (process 3 in Scheme 3) which is associated

SCHEME 3: Schematic Representation of the Main Relaxation Paths[a] for the D−A Biphenyls II and III after Excitation into a Manifold of Vibronic States

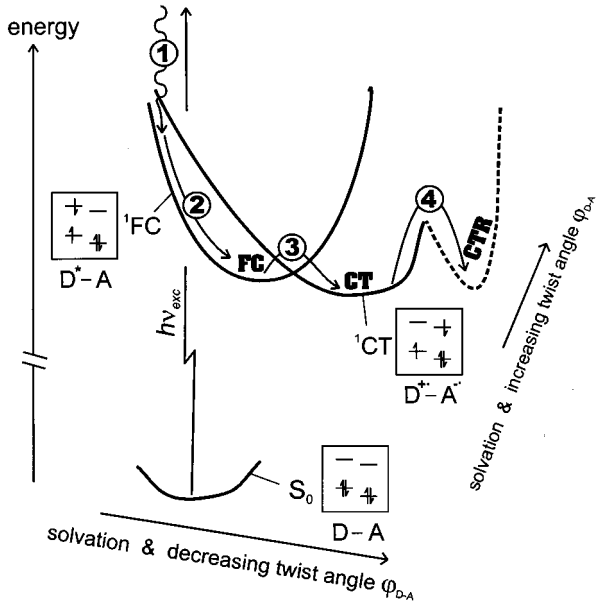

[a] (1) vibrational relaxation, (2) initial solvation and geometry relaxation toward a more planar structure than that in S_0, (3) ET interconversion, and (4) additional structural relaxation to a more twisted conformation than that in S_0 occurring only for **III**. The characteristic one-electron configurations (within a composite-molecule description of localized HOMO and LUMO orbitals of the linked D and A phenyl subunits) of the involved states S_0 (1^1A), ^{1}FC (1^1B) and ^{1}CT (2^1A) are shown in boxes.

TABLE 3: Parameters of the Solvents Used at 298 K and Time Constants $\tau_{FC\rightarrow CT}$ of the Charge-Transfer Processes Observed by Time-Resolved Transient Absorption for I−III

	polarity			solvent relaxation		$\tau_{FC\rightarrow CT}$ [ps]		
solvent	ϵ_r[a]	$f_2(\epsilon_r)$[b]	viscosity η [mPa s][a]	τ_l [ps]	τ_s[ps]	**I**	**II**	**III**
HEX	1.9	0.09	0.30			(2.2 ± 0.2)	(2.2 ± 0.2)	(2.2 ± 0.2)
EOE	4.3	0.25	0.22	<1.6[d]	<2.4[d]		(5.2 ± 0.4)	(5.7 ± 0.5)[g]
TAC	7.0[c]	0.30	≈15	≈150[e]	≈690[e]	(69 ± 17)	(64 ± 12)	(10 ± 1)
ACN	35.9	0.39	0.33	0.2[f]	0.4−0.9[f]	(2.5 ± 0.1)	(2.5 ± 0.1)	(6.0 ± 0.5)[g]

[a] References 49 and 50. [b] $f_2(\epsilon_r) = (\epsilon_r - 1)/(2\epsilon_r + 1) - (n^2 - 1)/(4n^2 + 2)$ from ref 51. [c] References 52 and 53. [d] Estimated from ethyl acetate;[17,54] in EOE τ_s and τ_l are expected to be considerably faster because the solvent viscosity of ethyl acetate ($\eta = 0.36$ mPa s) is larger than that of EOE ($\eta = 0.22$ mPa s). [e] τ_l is calculated in ref 55 by inverse Laplace transformation of Davidson−Cole data from ref 52; τ_s is taken from refs 52 and 56. [f] References 17−19, 53, and 56. [g] In **III** the CT process is superimposed by the structural relaxation to the **CTR** species.

with a partial electron transfer. The vibrational relaxation (process 1), on one hand, can be excluded since both kinetic species **FC** and **CT** possess completely different spectral features and, on the other hand, the intramolecur rotation toward a more planar geometry (process 2) can be excluded, because the model compound **I**, which is restricted to planarity, shows the same kinetic behavior as the flexible biphenyl **II**. In the following section, the possible rate-limiting factors of the $^1FC\rightarrow{}^1CT$ process are discussed.

4.2.1. Kinetics of State Interconversion $^1FC\rightarrow{}^1CT$. The observed relaxation times, $\tau_{FC\rightarrow CT}$, together with the relevant solvent parameters, are listed in Table 3. They reveal that the $^1FC\rightarrow{}^1CT$ processes of **I**−**III** are slower than solvation dynamics (the longitudinal solvent relaxation times τ_l or the related solvation times τ_s) in the fast relaxing solvents EOE and ACN. Let us first test the possibility to describe the interconversion with a low barrier ET reaction in the purely adiabatic regime.

A numerical treatment of the experimental relaxation times within (semi-)classical ET models[57,58] needs parameters, such as reorganization energy for the solvent (λ_s) and low-frequency intramolecular motions (λ_i'), the reaction free energy ΔG and activation barrier $\Delta G^{\#}$, as well as τ_l, which can only very crudely be determined. Best results can be obtained for ACN, since only for this solvent a reliable mean value (narrow distribution) of τ_l is known from various references.[17−19,53,56] The fact that $\tau_{FC\rightarrow CT} > 10t_l > \tau_s$ in ACN (Table 3) may allow us to apply transition-state ET theory which requires a quasi-equilibrium between precursor and transition state.[20,21] In the case of a purely adiabatic and solvent diffusion controlled ET reaction, the theoretical rate constant can then be calculated by[57]

$$\tau_{et}^{-1} = \frac{1}{\tau_l}\sqrt{\frac{\lambda_s}{16kT\pi}}e^{-\Delta G^{\#}/kT} \qquad (3)$$

This equation is derived from transition state theory including Kramers diffusion treatment for a relaxing Debye solvent.[57,59] It is practically equivalent to the result of the classical two-dimensional Sumi−Marcus model[26] (adiabatic limit without high-frequency vibrations) in the case of $\lambda_s > \lambda_i'$ and $\tau_{et} > \tau_s$ being appropiate for the conditions in the polar solvent ACN. The solvent reorganization energies λ_s may be determined from

$$\lambda_s = \frac{\Delta\mu^2}{a^3}\left(\frac{\epsilon - 1}{2\epsilon + 1} - \frac{n^2 - 1}{2n^2 + 1}\right) \qquad (4)$$

using the dipole moment differences $\Delta\mu = \mu_{CT} - \mu_{S0}$ and Onsager cavity radius $a = 6$ Å as obtained elsewhere[4] from Lippert−Mataga plots[51] (assuming $\mu_{S0} \approx \mu_{FC}$). Such estimates of λ_s for **I**−**III** in ACN are (1800 ± 700) cm^{-1}, (2000 ± 700) cm^{-1}, and (3600 ± 1500) cm^{-1}. The range of the resulting theoretical ET times of **I**−**III** according to eq 3 for a low barrier $\Delta G^{\#} = (170 \pm 90)$ cm^{-1} which has been given for the ET reaction in BA, are (1.1 ± 1) ps, (1.1 ± 1) ps, and (0.8 ± 1) ps. For comparison, using $\lambda_s = 3100$ cm^{-1} as reported for BA,[60] eq 3 yields 1 ps which is close to the experimental ET time τ_{et} in BA obtained by Barbara et al.[5] (0.75 ps) and close to the solvation time τ_s of ACN determined by time-dependent Stokes shift experiments.[17−19,53,56] By contrast, the observed rates $\tau_{FC\rightarrow CT}$ of **I**−**III** (Table 3) are even slower than the limits of the theoretical τ_{et} and also slower than τ_s. This indicates that the observed interconversion process $^1FC\rightarrow{}^1CT$ cannot be described by a low-barrier crossing and solvent-controlled adiabatic ET reaction as proposed previously.[2] Thus, we have to ask for another rate-limiting factor of the $^1FC\rightarrow{}^1CT$ process.

Within general ET theory, three reasons can be responsible for such a rate limitation: (i) a large amplitude motion, (ii) a thermal activation barrier $\Delta G^{\#}$ larger than kT, or (iii) a weak electronic coupling matrix element $V^1{}_{FC-1CT}$ in the order of 100 cm^{-1} or less.

(i) The possibility of a rate limitation due to a intramolecular rotation around the interannular bond can be excluded since **II** and the planar fluorene **I** possess equal $\tau_{FC\rightarrow CT}$ (2.2 ps in HEX and 2.5 ps in ACN). However, the observed lower rate of **III** in ACN is consistent with a temporal superposition of the large amplitude motion toward a more twisted structure (see Scheme 3). A strong influence of another motion including rotation of the dimethylaminogroup seems unlikely because the interconversion process is connected with a transfer of charge from the dimethylanilino donor to the benzonitrile acceptor group.

(ii) To conclude about the involvement of a thermal barrier, temperature dependent measurements are usually necessary. Rough estimates using classical ET theories (eq 3) and solvent continuum models (eq 4) indicate barriers at most in the order of kT which could hardly explain such low rates. Furthermore, the influence of the solvent polarity on $\tau_{FC\rightarrow CT}$ of **I**−**III** (Table 3) is weak in comparison to known intramolecular ET reactions.[23,40] This also contradicts a significant activation barrier $\Delta G^{\#}$.

(iii) Following the explanations in the preceding discussion chapters, where the two kinetic species **FC** and **CT** are assigned to two states of different zeroth-order symmetry (Scheme 3), an involvement of a weak electronic coupling matrix element $V^1{}_{FC-1CT}$ is favored. To test this idea, the one-electron matrix elements $\langle{}^1\Phi_{Lb}|H|{}^1\Phi_{CT}\rangle$ between the leading delocalized SCF electron configurations of $S_2(^1L_b)$ and $S_1(^1CT)$ are calculated using the ZINDO/S method[61] with a CI expansion of 122 single excitations. The obtained $\langle{}^1\Phi_{Lb}|H|{}^1\Phi_{CT}\rangle$ amounts to 185 cm^{-1} for **III** at the twist angle $\varphi = 70°$ and 30 cm^{-1} for **II** at $\varphi = 20°$. By introducing an increasing self-consistent reaction field to simulate the solvent polarity influence, $\langle{}^1\Phi_{Lb}|H|{}^1\Phi_{CT}\rangle$ of **III** continuously decreases down to 35 cm^{-1} (ACN conditions) due to an increasing energy gap between the leading configurations

^1L_b and ^1CT, while $\langle {}^1\Phi_{Lb}|H|{}^1\Phi_{CT}\rangle$ of **II** remains constant around (30 ± 5) cm^{-1}. Such low coupling matrix elements are indeed consistent with the observed slow interconversion rates from ^1FC to ^1CT. Moreover, the calculated larger coupling element of **III** could explain why the experimental time constant $\tau_{FC\rightarrow CT}$ in TAC is faster for **III**. Note that in the fast relaxing solvents EOE and ACN, $\tau_{FC\rightarrow CT}$ is slower for **III** than that for **II** because the structural relaxation of **III** superimposes the electronic relaxation which is kinetically separated only in the viscous solvent TAC. The fact that the processes $^1FC\rightarrow{}^1CT$ of **I**−**III** in TAC are considerably faster than solvent dynamics ($\tau_{FC\rightarrow CT} < \tau_s$ and τ_l)[52,56] and likewise faster than the ET of BA in TAC ($\tau_{et} = 750$ ps at 285 K)[5] further supports the view of a not purely adiabatic and not solvent-controlled reaction.

On the other hand, the comparison of the relaxation times $\tau_{FC\rightarrow CT}$ in the almost equipolar solvents EOE and TAC (Table 3) reveals that the rates are slowed by the solvent viscosity. This is, of course, due to a nonnegligible influence of solvent diffusion processes which mainly control adiabatic ET reactions ($\tau_{et} \propto \tau_s$). Therefore, it appears reasonable to characterize the observed charge-transfer processes as ET reactions between the adiabatic and nonadiabatic limit. For such border cases, eq 3 has been modified to[28,57]

$$\tau_{et}^{-1} = \frac{4\pi^2}{h}V^2\frac{1}{\sqrt{4\pi\lambda_s kT}}e^{-\Delta G^{\#}/kT}\frac{1}{1+\frac{8\pi^2V^2}{h\lambda_s}\tau_l} \qquad (5)$$

which considers the electronic coupling matrix element V as well as the solvent diffusional influence of τ_l. Using the same parameter for **II** in ACN as above and $\tau_{et} = 2.5$ ps, a sensible value for $V^1{}_{FC-{}^1CT}$ of 70 cm^{-1} is obtained by eq 5. However, it is important to stress, that the theoretical data derived for **I**−**III** in ACN, which rest on the continuum model, are just indicative and not expected to result in quantitative agreement. In addition, the fact that the observed rate constants in TAC are faster than the upper limit ($=\tau_l^{-1}$) of eq 5 indicates a possible acceleration by fast inertial solvent modes or intramolecular vibrational dynamics. Numerical simulations of time-dependent population distributions are necessary which include high-frequency intramolecular and inertial solvent modes within a quantum mechanical description[28−31,33] and which treat nonequilibrium solvation explicitly within a stochastic treatment.[8,26,27,32−34] However, because of strong spectral overlap and shift of bands, the present experimental results do not allow such a sophisticated analysis.

5. Conclusions

The intramolecular charge-transfer processes in the investigated donor−acceptor biphenyls after photoexcitation cannot be described using a single state which gradually relaxes from the Franck−Condon excited region to the charge transfer region on a nonperturbed potential surface governed only by solvation dynamics. On the time scale of a few picoseconds, two excited-state species (**FC** and **CT**) with different transient absorption and stimulated emission (gain) spectra have been observed linked by a precursor−successor relationship. The different spectral features, in particular the occurrence of dual gain bands, can also not be due to vibrational cooling,[62] but are well consistent with an electron transfer from a primary populated $\pi\pi^*$ state ^1FC in the Franck−Condon region to the charge transfer state ^1CT that has been analyzed previously.[1,3,4,9] The short-lived ^1FC state is characterized by the ^1L_b-type $S_2(1^1B)$ state which interacts with the close lying ^1L_a-type $S_1(^1CT)$ state. The $S_2(1^1B)$ nature of the precursor state ^1FC follows from three main conclusions: (i) In the less polar solvents, where the energy gap between the ^1FC ("1^1B") and lower lying ^1CT (2^1A) state is small, the gain of the primary species (**FC**) is weaker than that of the product species (**CT**). For high solvent polarity (acetonitrile, larger energy gap) there is even an absence of gain for the first species (**FC**) which can be explained by the reduced mixing with the allowed $1^1A\leftarrow{}^1CT(2^1A)$ transition.

(ii) By comparison with the steady-state absorption, as well as with quantum chemical (AM1/CI) calculations, the observed excited-state absorption bands can be assigned to the first-order transitions $S_2(1^1B)\rightarrow{}^1C_b(n^1B)$, $S_1(2^1A)\rightarrow{}^1C_a(n^1A)$ and $S_1(2^1A)\rightarrow{}^1L_a(3^1A)$. Consequently, the observed gain bands are correlated with the stimulated fluorescence transitions $S_0(1^1A)\leftarrow S_2(1^1B)$ and $S_0(1^1A)\leftarrow S_1(2^1A)$. However, because of the high oscillator strength necessary for the observation of gain for this ^1FC state together with the polarity induced shifts of absorption and gain bands, ^1FC cannot be regarded as a pure ^1L_b state but better as a state with mixed $^1L_b/{}^1CT$ ($1^1B/2^1A$) character.

(iii) The observed rates for the charge-transfer process $^1FC\rightarrow{}^1CT$ of **I**−**III** in the fast relaxing aprotic solvents are considerably slower than the characteristic solvent relaxation times τ_s and also slower as compared to the ET rates observed for other typical biaryl compounds, such as 9,9′-bianthryl,[5,7] ADMA,[8] 9DPhen,[14] and their derivatives. This suggests that beside conformational dynamics of **III**, the different symmetry of the precursor and successor states, which holds only in the biphenyl series, is responsible for an additional rate reduction through a small electronic interaction matrix element.

Due to the strong spectral changes on the time scale of ET, **I**−**III** can be regarded as illustrative model systems for an intramolecular electron transfer of case B (i.e., ET between two distinct states with considerably less solvent than intramolecular control). Our observations are in line with recent reinvestigations on the well-known laser dyes DCM (4-dicyanomethylene-2-methyl-6-p-dimethylaminostyryl-4H-pyran),[36,37] C153 (coumarin 153),[38,39] and DCS (4-dimethylamino-4′-cyanostilbene)[63,64] in polar solvents. On a femto- to subpicosecond time scale, the ^1CT state is fed by different precursor states, the electronic structure of which could, however, not be characterized in such a detail as for **I**−**III**.

Concerning the conformational dynamics of **II** and **III**, this study gives additional support to the conclusions derived previously from time-resolved emission[4,9,10] and allows to go into more detail regarding the conformer species (**CT** and **CTR**) involved the following: a relaxation toward planar conformers (**CT**) is observed for **II** in all solvents and **III** in nonpolar *n*-hexane as demonstrated by the similarity of the spectral and kinetic behavior as the compound **I** which is restricted to planarity. In medium polar solvents, the initial relaxation of **III** toward planarity is followed by a viscosity controlled rearrangement toward a more twisted structure (**CTR**) as shown by further spectral evolutions after the ET process. In strongly polar acetonitrile, the acceleration of the conformational relaxation to the **CTR** species leads to a temporal superposition with the ET interconversion $^1FC\rightarrow{}^1CT$ such that the observable overall charge-transfer rate is reduced and **CTR** is directly observed as the product species. The final transient spectrum resembles the sum of dimethylaniline (D) cation and benzonitrile (A) anion spectra which indicates the strong decoupling of the D and A submoieties in the **CTR** species of **III** most probably by a nearly perpendicular twist.

All spectral, kinetic, and conformational aspects can be summarized in a three excited-state species (two electronic

states) model (Scheme 3) for the investigated donor−acceptor biphenyls: **FC** ($^{\prime\prime}{}^1L_b/{}^1CT^{\prime\prime}$) → **CT** (^{1}CT) → **CTR** (^{1}CT). After the photoinduced population of the ^{1}FC state appears, the reaction to the ^{1}CT state takes place in all biphenyls **I**−**III** connected with a charge separation between the phenyl units and a more planar geometry than in the ground state. In addition, the subsequent adiabatic photoreaction to a more relaxed (more twisted and more polar) **CTR** species occurs only for the pretwisted compound **III** in dipolar solvents.

Acknowledgment. We are grateful for the travel support by the Deutscher Akademischer Austauschdienst DAAD (Procope Project). M.M. thanks the Deutsche Forschungsgemeinschaft (DFG Projects Re 387/9-1 and Re 387/9-2) for financial support.

References and Notes

(1) Lahmani, F.; Breheret, E.; Zehnacker-Rentien, A.; Amatore, C. and Jutand, A., *J. Photochem. Photobiol.* **1993**, *70*, *39*.

(2) Lahmani, F.; Breheret, Benoist d'Azy, O.; Zehnacker-Rentien, A; Delouis, J. F. *J. Photochem. Photobiol.* **1995**, *89*, 191.

(3) Maus, M., Rettig, W. *Chem. Phys.* **1997**, *218*, 151.

(4) Maus, M., Rettig, W., Bonafoux, D.; Lapouyade, R. *J. Phys. Chem. A* **1998**. To be submitted for publication.

(5) (a) Kahlow, M. A.; Kang. T. J.; Barbara, P. F. J. *Phys. Chem.* **1987**, *91*, 6452. (b) Barbara, P. F.; Jarzeba, *W. Acc. Chem. Res*. **1988**, *21*, 195.

(6) Kang, T. J.; Jarzeba, W.; Barbara, P. F.; Fonseca, T. *Chem. Phys.* **1990**, *149*, 81.

(7) Mataga, N.; Nishikawa, S.; Okada, T. *Chem. Phys. Lett.* **1996**, *257*, 327.

(8) (a) Tominaga, K.; Walker, G. C.; Jarzeba, W.; Barbara, P. F. *J. Phys. Chem*. **1991**, *95*, 10475. (b) Tominaga, K.; Walker, G. C.; Kang, T. J.; Barbara, P. F. *J. Phys. Chem.* **1991**, *95*, 10485.

(9) Maus, M.; Rettig, W.; Lapouyade, R. *J. Inf. Rec.* **1996**, *22*, 451.

(10) Rettig, W.; Maus, M.; Lapouyade, R. *Ber. Bunsen-Ges. Phys. Chem.* **1996**, *100*, 2091.

(11) Mataga, N.; Yao, H.; Okada, T.; Rettig, W. *J. Phys. Chem*. **1989**, *93*, 3383.

(12) Lueck, H.; Windsor, M. W.; Rettig, W.; *J. Phys. Chem.* **1990**, *94*, 4550.

(13) Onkelinx, A.; De Schryver, F. C.; Viane, L.; Van der Auweraer, M.; Iwai, K.; Yamamoto, M.; Ichikawa, M.; Masuhara, H.; Maus, M.; Rettig, W. *J. Am. Chem. Soc.* **1996**, *118*, 2892.

(14) Onkelinx, A.; Schweitzer, F.; De Schryver, F. C.; Miyasaka, H.; Van der Auweraer, M.; Asahi, T.; Masuhara, H.; Fukumura, H.; Yashima, A.; Iwai, K. *J. Phys. Chem. A* **1997**, *101*, 5054.

(15) Okada, T.; Mataga, N.; Baumann, W.; Siemarczuk, A. *J. Phys. Chem.* **1987**, *91*, 4490.

(16) Weaver, M. J., *Chem. Rev*. **1992**, *92*, 463.

(17) Rossky, P. J.; Simon, J. D. *Nature* **1994**, *370*, *263*.

(18) Weaver, M. J.; McManis, G. E., *III. Acc. Chem. Res.* **1990**, 23, 294.

(19) Maroncelli, M.; MacInnis, J.; Fleming, G. R. *Science* **1988**, 243, 1674.

(20) Barbara, P. F.; Meyer, T. J.; Ratner, M. A. *J. Phys. Chem.* **1996**, *100*, 13148.

(21) Yoshihara, K.; Tominaga, K.; Nagasawa, Y. *Bull. Chem. Soc. Jpn.* **1995**, *68*, 696.

(22) Takagi, Y.; Sumitani, M.; Yoshihara, K. *Rev. Sci. Instrum*. **1981**, 52, 1003.

(23) Schuddeboom, W.; Jonker, S. A.; Warman, J. M.; Leinhos, U.; Kühnle, W.; Zachariasse, K. A. *J. Phys. Chem*. **1992**, *96*, 10809.

(24) Rotkiewicz, K.; Grabowski, Z. R.; Jasny, J. *Chem. Phys. Lett.* **1975**, *34*, 55.

(25) Smith, M. J.; Krogh-Jespersen, K.; Levy, R. M. *Chem. Phys.* **1993**, *171*, 97.

(26) Sumi, H.; Marcus, R. A. *J. Chem. Phys.* **1986**, *84*, 4894.

(27) Nadler, W.; Marcus, R. A. *J. Chem. Phys*. **1987**, *86*, 563.

(28) (a) Jortner, J.; Bixon, M. *J. Chem. Phys.* **1988**, *88*, 167. (b) Bixon, M.; Jortner, *J. Chem. Phys.* **1993**, *176*, 467.

(29) Walker, G. C.; Akesson, E.; Johnson, A., E.; Levinger, N. E.; Barbara, P. F. *J. Phys. Chem.* **1992**, *96*, 3728.

(30) Akesson, E.: Johnson, A. E.; Levinger, N. E.; Walker, G. C.; DuBruil, T. P.; Barbara, P. F. *J. Chem. Phys.* **1992**, *96*, 7859.

(31) Kandori, H.; Kemnitz, K.; Yoshihara, K.*J. Phys. Chem*. **1992**, *96*, 8042.

(32) Schenter, G. K.; Duke, C. B. *Chem. Phys. Lett.* **1991**, *176*, 563.

(33) (a) Hynes, J. T., *J. Phys. Chem.* **1986**, *90*, 3701. (b) Fonseca, T.; Kim, H. J.; Hynes, J. T. *J. Mol. Liq.* **1994**, *60*, 161.

(34) Polimeno, A.; Barbon, P. L.; Nordio, P. L.; Rettig, W. *J. Phys. Chem.* **1994**, *98*, 12158.

(35) (a) Horng, M. L.; Gardecki, J. A.; Papazyan, A.; Maroncelli, M. *J. Phys. Chem.* **1995**, *99*, 17311. (b) Reynolds, L.; Gardecki, J. A.; Frankland, S. J. V.; Horng, M. L.; Maroncelli, M. *J. Phys. Chem*. **1996**, *100*, 10337.

(36) van der Meulen, P.; Zhang, H.; Jonkman, A. M.; Glasbeek, M. *J. Phys. Chem.* **1996**, *100*, 5367−5373.

(37) Kovalenko, S. A.; Ernsting, N. P.; Ruthmann, J. *Chem. Phys. Lett.* **1996**, 258, 445.

(38) Kovalenko, S. A.; Ruthmann, J.; Ernsting, N. P. *Chem. Phys. Lett.* **1997**, 271, 40.

(39) Jiang, Y.; McCarthy, P. K.; Blanchard, G. J. *Chem. Phys*. **1994**, 183, 249.

(40) Martin, M. M.; Plaza, P.; Changenet, P.; Meyer, Y. H. *J. Photochem. Photobiol. A* **1997**, *105*, 197.

(41) Agmon, C. *J. Phys. Chem*. **1990**, *94*, 2959.

(42) Dumon, P.; Jonusauskas, G.; Dupuy, F.; Pée, P.; Rulliére, C.; Létard, J. F.; Lapouyade, R. *J. Phys. Chem.* **1994**, *98*, 10391.

(43) AMPAC 5.0; Semichem, 7128 Summit, Shawnee, KS 66216 1994. Dewar, M. J. S.; Zoebisch, E. G.; Healy, E. F.; Stewart, J. P. *J. Am. Soc. Chem.* **1985**, *107*, 3902.

(44) (a) Elsaesser, T.; Kaiser, W. *Annu. Rev. Phys. Chem*. **1991**, *42*, 83. (b) Foggi, P.; Pettini, L.; Santa, I.; Righini, R.; Califano, S. *J. Phys. Chem*. **1995**, *95*, 7439.

(45) (a) Rulliére, C., *Can. J. Phys*. **1984**, *62*, 73. (b) Rulliére, C.; Joussot-Dubien, *J. Rev. Phys. Appl*. **1979**, 14, 303. (c) Rulliére, C. Ph.D. Thesis, University of Bordeaux, 1977.

(46) Shida, T. *Electronic Absorption Spectra of Radical Ions*; Elsevier Science Publishers B. V.; Amsterdam, 1988.

(47) (a) Shida, T.; Iwata, S. *J. Am. Chem. Soc*. **1973**, *95*, 3473. (b) Yoshihara, K.; Yartsev, A.; Nagasawa, Y.; Kandori, H.; Douhal, A.; Kemnitz, K. In *Ultrafast Phenomena VIII*. Martin, J.-L.; Migus, A.; Zewail, A. H.; *Springer Series in Chemical Physics*; Springer-Verlag: Berlin, 1993; Vol. 55, p 571.

(48) (a) Shida, T.; Haselbach, E.; Bally, T. *Acc. Chem. Res.* **1984**, *17*, 180. (b) Chutny, B.; Swallow, A. *Trans. Faraday Soc.* **1970**, *66*, 2847.

(49) Riddick, J. A.; Bunger, W. B.; Sakano, T. K. *Organic Solvents*; John Wiley & Sons: New York, 1986.

(50) Schäfer, K. H., Ed.*Landolt-Börnstein, Zahlenwerte und Funktionen aus Physik, Chemie, Astronomie, Geophysik und Technik*; Landolt-Börnstein, New series IV/6; Springer-Verlag: Berlin,1969; Vol. 2, no. 5.

(51) Liptay, W. In *Excited States*; E. C., Lim, Ed.; Academic Press: New York 1974; pp 129.

(52) Ras, A. M.; Bordewijk, P. *Recl. Trav. Chim. Pay-Bas* **1971**, *90*, 1055.

(53) Pöllinger, F.; Heitele, H.; Michel-Beyerle, M. E.; Anders, C.; Futscher, M.; Staab, H. A. *Chem. Phys. Lett.* **1992**, *198*, 645.

(54) Simon, J. D. *Acc. Chem. Res*. **1988**, *21*, 128.

(55) Braun, D. Ph.D. Thesis, Humboldt-University, Berlin, 1995. Published as Braun, D. *Fluoreszenzspektroskopische und theoretische Aspekte photoinduzierter intramolekularer Elektronentransferreaktionen und ihre Wechselwirkung zur Lösungsmittelumgebung*; Wissenschaftliche Schriftenreihe Chemie 30; Verlag Dr. Köster: Berlin, 1995 (ISBN 3-89574-119-1).

(56) Barbara, P. F.; Jarzeba, W. *Ultrafast Photochemical Intramolecular Charge and Excited-State Solvation*; Advances in Photochemistry 15; John Wiley & Sons: New York, 1990.

(57) Rips, I.; Jortner, J. *J. Chem. Phys.* **1987**, *133*, 411.

(58) Marcus, R. A.; Sutin, N. *Biochim. Biophys. Acta* **1985**, *811*, 265.

(59) Kramer, H. A. *Physica (Amsterdam)* **1940**, 7, 284.

(60) Schütz, M.; Schmidt, R. *J. Phys. Chem.* **1996**, *100*, 2012.

(61) ZINDO/S SCF/CI program package available from Zerner, M. C. University of Florida, Gainesville, FL. See: Zerner, M. C.; Loew, G. H.; Kirchner, R. F.; Mueller-Westerhoff, U. T. *J. Am. Chem. Soc.* **1980**, *102*, 589.

(62) We are currently investigating whether the population of the relaxed nonpolar precursor state (^{1}FC) depends on the excitation wavelength. Preliminary time-resolved polarization experiments verified a short-time component by excitation at 300 nm, while excitation at the red edge of the absorption spectra (360 nm) of **I**−**III** indicate a different decay mechanism which might be connected with direct population of the solvent relaxed CT species.

(63) E. Abraham, E.; Oberle, J.; Jonusauskas, G.; Lapouyade, R.; Rulliere, C. *Chem. Phys.* **1997**, 214, 409.

(64) Eilers-König, N.; Kühne, T.; Schwarzer, D.; Vöhringer, P.; Schroeder, J. *Chem. Phys. Lett.* **1996**, 253, 69.